

Speckle Interferometry Measurements of STF 1670 AB and STF 919 AB, AC, BC

Ethan Wuthrich¹ and Richard Harshaw²

1. Basha High School, Chandler, AZ.
2. Brilliant Sky Observatory, Cave Creek, AZ.

Abstract Historically, speckle interferometry has been the domain of large professional telescopes. This project demonstrated the use of amateur class equipment for use in speckle interferometry analysis. Star systems analyzed were STF1670AB (WDS 12417-0127) and STF919AB, AC, BC (WDS 06288-0702), where STF1670AB is a well-known visual binary system used in part to validate the methods used in this project. The angular separation (θ) and arc second separation (ρ) were measured and compared to historical records for these star systems. The data for the project was collected with a Celestron C-11 telescope and a high-speed CCD camera and processed using software REDUC 4.47 and Plate Solve 3.31. The θ and ρ values for the star systems were then calculated and recorded.

Introduction

Binary stars consist of two stars bound together by their gravity. The stars share an elliptical orbit, which can have an orbital period lasting anywhere from five minutes to thousands of years (Argyle 2012). As these stars orbit one another, their position in the sky relative to Earth changes. Accurate knowledge of the positions of stars in the night sky allows for the construction of accurate maps and time-keeping instruments (Pickering 1923). Much as ancient mariners used maps of the night sky to travel across the oceans, modern satellites use maps of the night sky to report their positions in their orbits around Earth. In order to keep the satellites in their proper orbits, the star maps must be updated through constant observation. Data collected by both amateur and professional astronomers is collected and tracked in catalogs, such as the Washington Double Star Catalog (WDS), and eventually used to determine the true orbits of the stars within a system. Once the true orbit is calculated, the data can then be used to determine the masses of the stars within the system, if the distance is known, and further refine the Hertzsprung–Russell (HR) diagram.

The three major methods of binary star observation are astrometry, photometry, and spectroscopy (Genet 2015). Within the field of astrometry, there is a method known as speckle interferometry. Speckle interferometry is the use of a very short exposure time of a star to reduce the effects of atmospheric seeing. Atmospheric seeing is the distortion of light from stars caused by turbulence within the Earth's atmosphere. This effect is what causes a star to appear to twinkle to the naked eye. A single session of data collection for speckle interferometry can produce thousands of images. A single image of the star is distorted (see Figure 1), but this data can be analyzed using the Fourier method (Labeyrie 1970) to create an autocorrelogram, which can then be used to calculate the angular separation (θ) and arc second separation (ρ).

Observations for this paper were obtained at the Brilliant Sky Observatory located at Cave Creek, Arizona USA (see Figure 2 below) on 2015 February 18th (2015.13) and 2015 April 13th (2015.28). Additional observations were made in the Arizona desert approximately 120 miles west of Phoenix, Arizona on 2015 February 11th (2015.276).



Figure 1: Single frame image of STF919A, B, C, taken 2015 Feb 18 at Brilliant Sky Observatory located at Cave Creek, Arizona USA



Figure 2: Ethan Wuthrich and Richard Harshaw at Brilliant Sky Observatory, Cave Creek, AZ

In this investigation, speckle interferometry was used to determine the current positions of the stars in the star systems STF1670AB (WDS 12417-0127) and STF919AB, AC, BC (WDS 06288-0702), to better understand their positions in the night sky.

Equipment and Software Used

The equipment used during observation consisted of a Celestron C-11 (11-inch SCT telescope) on an equatorial mount, equipped with a 5x PowerMate (used for f/50 observations) or a 2.5x PowerMate (used

for f/25 observations), a Johnson-Cousins R Filter, a flip mirror, a Digital Focus Counter, and a Skyris 618C high speed camera. Data from the Skyris camera was captured using FireCapture software on a 64-bit computer to capture the video images as avi (Audio Video Interleave) files.

The avi files obtained during the observations were processed using two software packages: REDUC 4.74, by Florent Losse, to convert avi files to FITs; and Plate Solve 3.31, by David Rowe of PlainWave Instruments, to pre-process the FITs files to PSD files and to do the speckle analysis to create the autocorrelogram used to obtain measurements for rho and theta (see example in Figure 3).

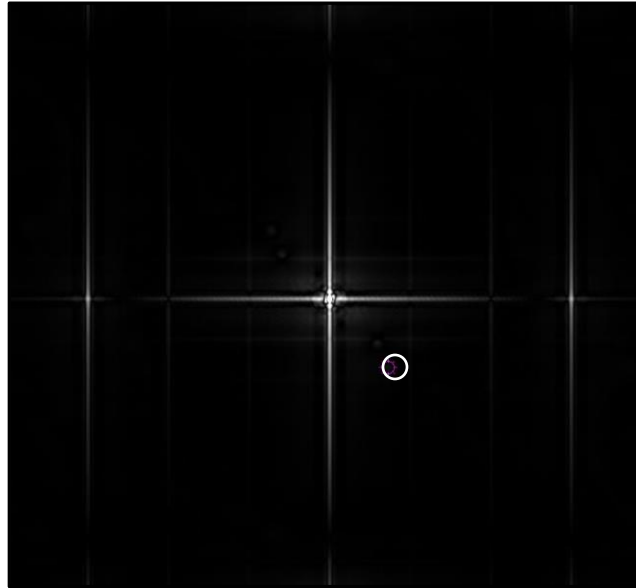


Figure 3: STF919A, B, and C autocorrelogram created using PlateSolve 3.31

Picking a Star System for Observation

Selecting a star system to observe is based on the specifications of the telescope being used, expected seeing conditions on the night of observation, the magnitudes of both the primary and component stars, and their separation. After some trial and error, it was found that a good guideline for this system were stars that had a separation between 2 and 5", with the primary star's magnitude (PMag) ≤ 7 and the companion star's magnitude (CMag) ≤ 7 , but not substantially dimmer than Pmag (to prevent washout of the companion star by the primary star). For viewing in Cave Creek, Arizona, a star system should have declination $\geq -26^\circ$, and be as close to celestial meridian as possible at the time of observation. Table 1 shows an abbreviated summary of the systems chosen for observation from the WDS catalog.

WDS	Dis Comp	First	Last	Nob	PAF	PAL	SF	SL	VMagP	VMagS	Coord
12417-0127	STF1670AB	1720	2013	1593	319	10	7.5	1.9	3.48	3.53	124139.60-012657.9
06288-0702	STF 919AB	1822	2013	127	130	133	6.9	7	4.62	5	062849.07-070159.0
06288-0702	STF 919AC	1777	2013	55	139	126	9	10	4.62	5.39	062849.07-070159.0
06288-0702	STF 919BC	1822	2013	134	101	108	3.2	3	5	5.32	062849.42-070204.0

Table 1: Summary of star systems observed

Initially the BC pair from STF 919 was chosen, but the observations included the A component star, and data gathered for all three combinations was a natural result of the process. See Figure 4, Stacked Frame Image, showing all 3 component stars A, B, and C of STF 919.

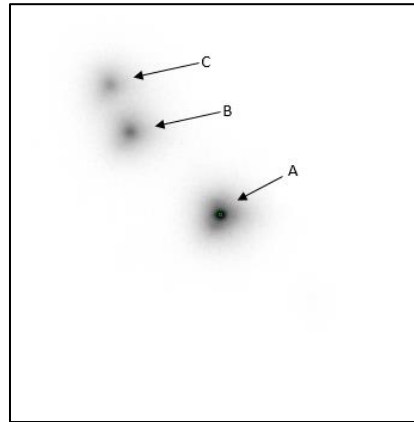


Figure 4: Stacked frame image of STF919 A, B, and C created using REDUC 4.74.

Pixel Scale Calibration

Calibration of the camera used to capture images during observations is critical in obtaining correct measurements for the star systems being observed. Calibration is the process by which one determines the size of each camera pixel in arc seconds, referred to as the image scale, or plate scale. The plate scale is not just dependent on the camera, but also on the focal length of the telescope and the entire optical path. For example, the plate scale for the telescope set up at $f/25$ is different than the plate scale for the telescope set up at $f/50$. Any change in the optical path changes the plate scale, and calibration will need to be repeated with any change.

A substantial amount of work went into the calibration of the Skyris 618C high speed camera, with some help by other students on the Arizona team. Several methods were used to determine the plate scale for both the $f/25$ and $f/50$ setups (Harshaw 2015). Table 2 shows a summary of the methods used to calibrate the camera.

Camera Angle Calculation

Camera angle is the angle that the camera is mounted onto the telescope with respect to true celestial north. Since the method used to connect the camera is to insert the circular optical tube of the camera into a circular mount, the camera is at a different angle with respect to celestial north each time the camera is mounted onto the telescope. Thus for every set of observations, there is a need to gather a drift exposure. The drift exposure is obtained by moving the image of a star to one side of the screen, and then to turn the tracking motor of the telescope off, so the telescope does not move. This will allow the star to drift across the field of view of the camera from east to west across the screen. Once the star is past the field of view, one turns the tracking motor back on, all the time recording the event. This drift method can then be used to determine the angle of the camera at the time of observation.

Because of the distorted nature of the individual frames caused by upper atmospheric turbulence and its impact on astronomical seeing, multiple analyses were done to calculate an average drift angle. The drift avi files were split with REDUC into the individual frames, which were then saved as BMP (Bitmap) files. The BMP files were then loaded into REDUC to use the Drift Analysis function. As part of this, a beginning frame (Comp A) and an ending frame (Comp B) were selected and then the Drift Analysis function was executed. The Drift Analysis function computed an angle based on the center of the star system in the Comp A frame and the Comp B frame.

Method	Value of "e"	Weight	Wtd Total	Wtd Mean
f/10 H-Alpha 12mm Grating	0.375	4.000	1.500	0.375
f/10 H-Alpha Bahtinov Mask	0.372	4.000	1.488	
f/25 drift tests	0.162	0.250	0.041	0.153784314
f/25 Gamma Leonis	0.141	2.000	0.282	
f/25 Green Laser 12mm Grating	0.156	4.000	0.624	
f/25 H-Alpha 12mm Grating (1)	0.156	4.000	0.624	
f/25 H-Alpha 12mm Grating (2)	0.156	4.000	0.624	
f/25 H-Alpha 6mm Grating	0.154	4.000	0.616	
f/25 H-Alpha Bahtinov Mask	0.155	4.000	0.620	
f/25 O-III 12mm Grating	0.092	0.250	0.023	
f/25, 7 CPM stars	0.156	3.000	0.468	
f/50 drift tests	0.076	0.250	0.019	
f/50 Gamma Virginis	0.069	2.000	0.138	
f/50 Green Laser 12mm Grating	0.069	4.000	0.276	
f/50 H-Alpha 12mm Grating (1)	0.069	4.000	0.276	
f/50 H-Alpha 12mm Grating (2)	0.069	4.000	0.276	
f/50 H-Alpha 6mm Grating	0.069	4.000	0.276	
f/50 H-Alpha Bahtinov Mask	0.068	4.000	0.272	
f/50 O-III 12mm Grating	0.041	0.250	0.010	
f/50 STF 1523 AB	0.074	2.000	0.148	
f/50, 7 CPM stars	0.069	3.000	0.207	

Table 2: Summary of calibration methods

Report on STF1670AB

The star system STF1670AB (WDS 12417-0127) was observed on the night of April 11, 2015, at a focal setting of f/25 with a total of five exposures consisting of 1000 frames each. A dark frame was also taken with the f/25 setup to remove background noise during processing. A drift exposure of STF1670AB was taken to determine the camera angle. The camera setup was then changed to a focal length of f/50, and STF1670AB was observed with three exposures consisting of 1000 frames each. A dark frame was again taken with the f/50 setup. An exposure of nearby Spica was taken for use as a deconvolution star for the f/25 and f/50 exposures. Also, a drift exposure of Spica was taken with the f/50 setup to be used to determine the camera angle for the f/50 setup.

Both sets of exposures were converted to FITS cubes using REDUC and analyzed using Plate Solve 3 to determine the values of rho and theta. Due to the difficulty of obtaining an exact calibration of the pixel scale for both the f/25 and the f/50 setups, multiple calculations in Plate Solve 3 were used on each FITS cube to determine rho and theta. Plate Solve analysis was also done on the f/25 and f/50 data sets, both with and without the dark exposures.

In order to obtain a best estimate of the drift angle, for both the f/25 and f/50 setups, the drift files were analyzed in REDUC by making multiple drift analyses for each respective file, varying the beginning and ending frames used for each analysis. Forty different calculations were done on the f/25 drift file and 36 calculations were done on the f/50 Spica drift file, in order to obtain a statistically sound camera angle based on the mean value of each set of calculations.

STF1670AB was again observed on April 13, 2015 at Brilliant Sky Observatory, with five separate exposures at f/50, a dark exposure, a deconvolution star exposure, and a drift angle exposure. The PSD files were analyzed in Plate Solve 3.

Multiple STF1670AB estimates of rho and theta were calculated with both the f/25 and f/50 data sets using the Speckle Reduction function in Plate Solve 3. Estimates for the camera plate scale (E) were based on the calibration methods mentioned above in Table 2, combined with multiple focal lengths as shown below in Table 3 (green laser with grating with a f/25 E value of 0.137"/pixel and a f/50 E value of 0.0605"/pixel). CPM pair analysis yielded an E value of 0.1558"/pixel at f/25 and an E value of 0.0686"/pixel at f/50.

During the five f/25 observations made on 4/11/15, rho and theta values were estimated using the 0.137"/pixel green laser calibration value, both with and without the dark exposure subtractions. Rho and theta for the f/25 were again calculated using the CPM pairs calibrated values of E with the dark exposure subtractions.

The f/50 observation set consisted of three exposures taken on 4/11/15 and five taken on 4/13/15. Rho and theta estimates were made using three different calibration values: the green laser calibration, an estimate calibration based on a delta between the f/25 green laser calibration and the f/25 CPM pair calibrations, and finally the f/50 CPM pair calibrations.

Observation Date	f	Field Observations	Green Laser	Green Laser (Dark)	f/25 CPM Pairs	f/50 observations using 'E' estimates from f/25 CPM Pair Observations	f/50 CPM Pairs
4/11/2015	f/25	5	x		x		
4/11/2015	f/50	3	x	x		x	x
4/13/2015	f/50	5	x	x	x	x	x

Table 3: Summary of focal lengths and calibration combinations for STF1670

Camera angle, Δ , calculated for the f/25 observation was 6.334° based on 40 separate drift angle calculations. The results are displayed in Figure 5.

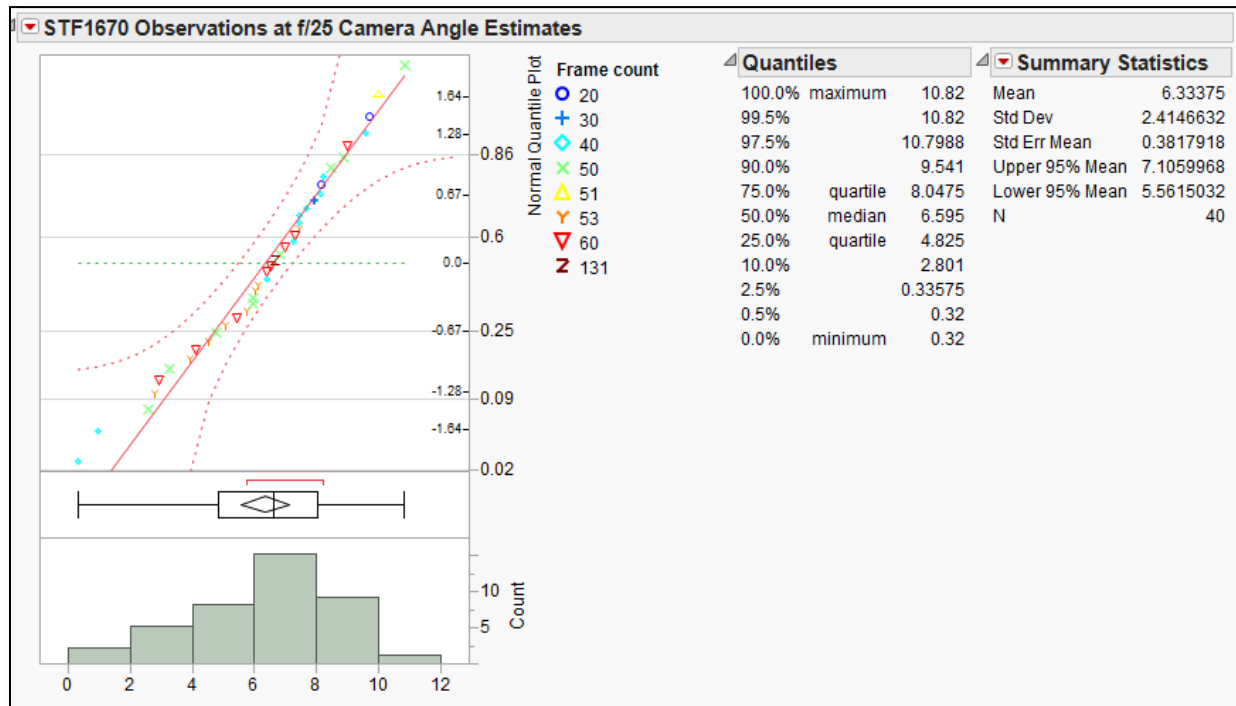


Figure 5: Plot of April 11, 2015 f/25 observation camera angle estimates.

Drift angle calculated for the f/50 observation was -21.048° based on 36 separate drift angle calculations. The results are displayed in Figure 6.

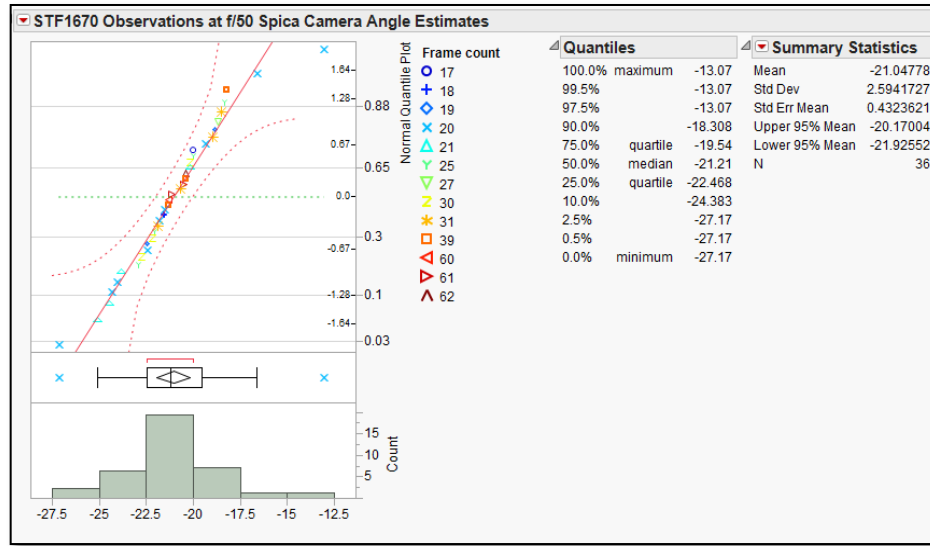


Figure 6: Plot of April 11, 2015 f/50 observation camera angle estimates.

STF1670AB Plate Solve residuals

The residuals for both the f/25 and f/50 rho and theta estimates done in Plate Solve 3 were then analyzed in JMP™ statistical software (JMP®, Version 12.0.1. SAS Institute Inc., Cary, NC, 1989-2007), and plotted with the historical WDS data to create an orbital plot (Figures 7 and 8) and an orbital period plot of rho (Figures 9 and 10). The mean rho and theta values of the focal length calibration combinations are shown in Table 4. Using the orbital period plot of rho and the WDS historical data from 2006 to 2015, a quadratic line was fit to the historical data and extrapolated through the data estimates for rho. The RSquare value for the fitted line was 0.9887. Based on this plot, the CPM methodology of calibration was the most accurate. Specifically, the f/25 observation made on 4/11/15, combined with the f/25 CPM calibration e values, gives a mean theta value of 4.961° and a mean rho value of 2.193".

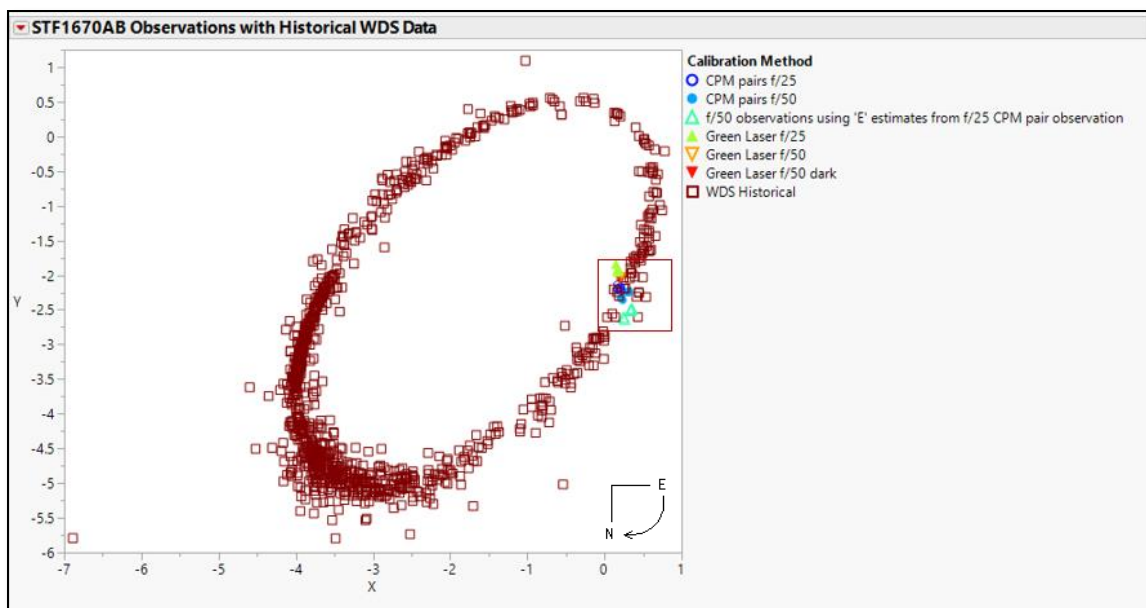


Figure 7: Plot of STF1670AB 4/11/15 and 4/13/15 observations by calibration method with historical WDS data.

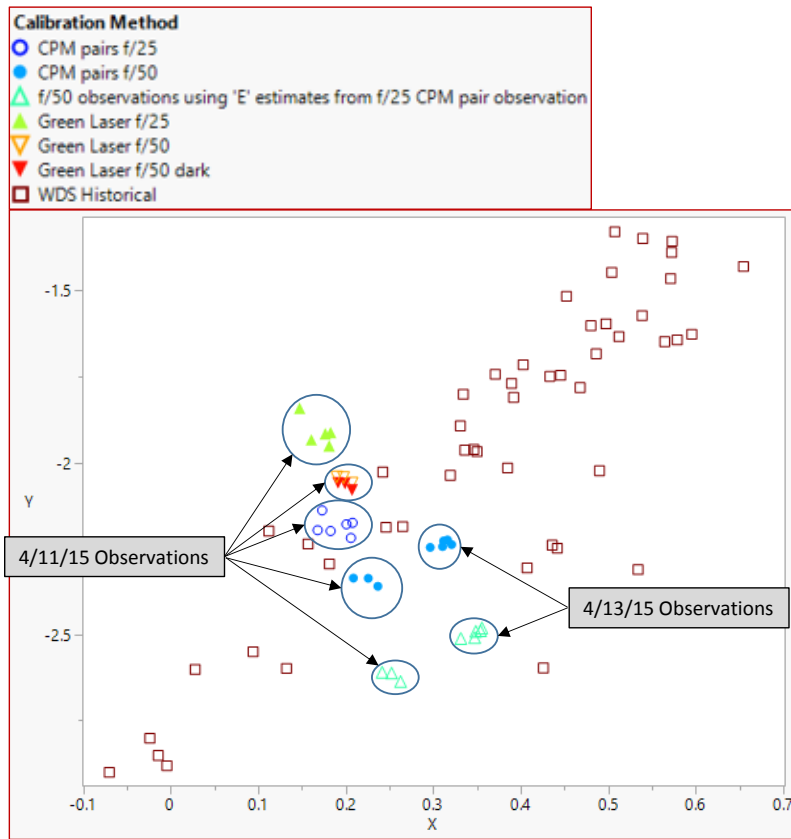


Figure 8: Plot of STF1670AB 4/11/15 and 4/13/15 observations by calibration method with historical WDS data.

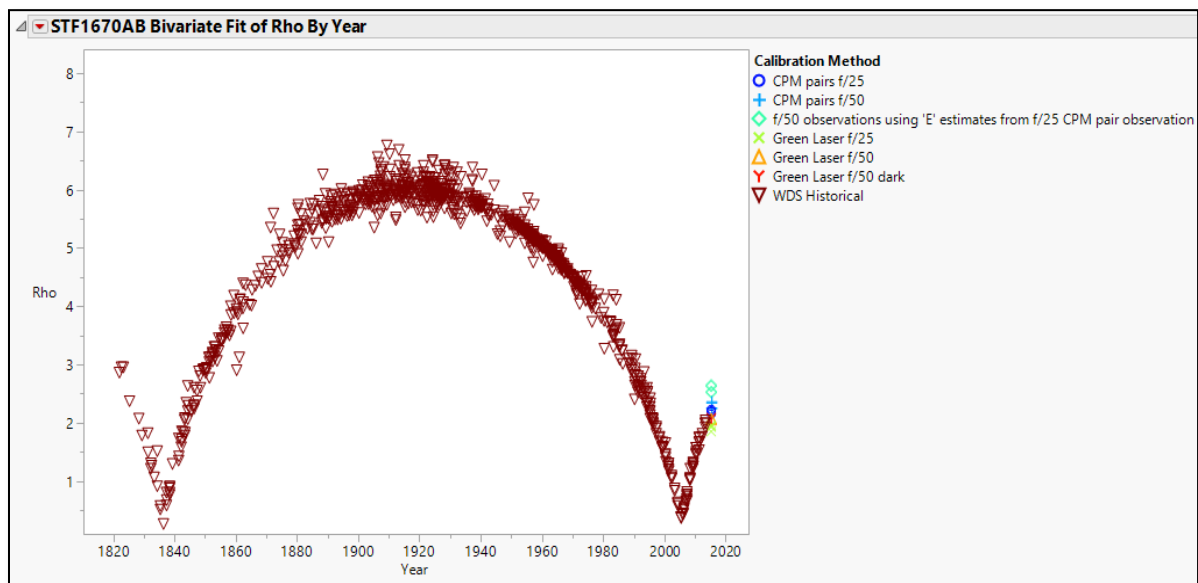


Figure 9: 169 Year Orbital Period rho Plot of STF1670AB 4/11/15 and 4/13/15 observations by calibration method with historical WDS data.

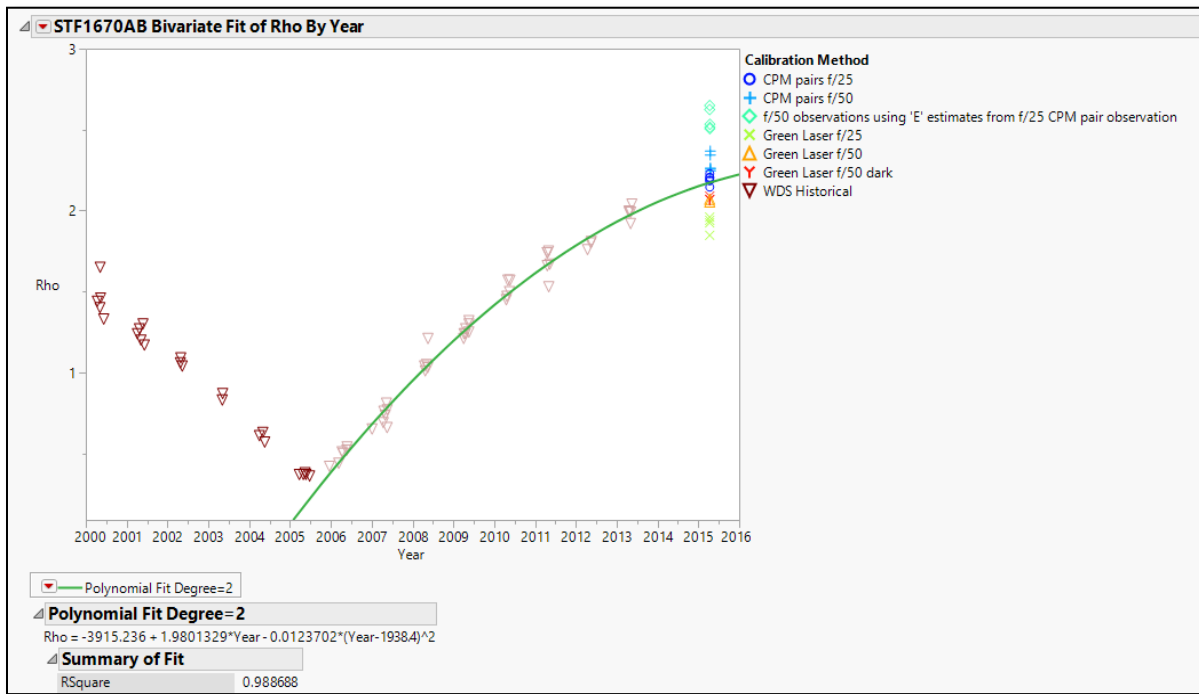


Figure 10: Orbital period rho plot of STF1670AB 4/11/15 and 4/13/15 observations by calibration method with historical WDS data. Line of best fit added to WDS observations from 2006 to 2015.

Calibration Method	Mean(Rho)	Mean(Theta)
CPM pairs f/25	2.1928	4.9605
CPM pairs f/50	2.2941	6.9948
f/50 observations using 'E' estimates from f/25 CPM pair observation	2.5589	7.1084
Green Laser f/25	1.9187	5.0676
Green Laser f/50	2.0554	5.5212
Green Laser f/50 dark	2.0759	5.5030

Table 4: Summary of STF1670AB theta and rho calculations based on calibration method.

Report on STF919AB, AC, BC

The star system STF919 was observed on the night of 2015 Feb 18, at Brilliant Sky Observatory, with the telescope focal length setup at f/50. Twelve separate exposures of 1000 frames each were taken. After the 12 exposures, seeing conditions became poor due to clouds and haze in the area of STF919, and Rigel was selected to be used for the drift exposure to determine camera angle, and another Rigel exposure was taken to be used for deconvolution during analysis.

STF919 was again observed on the night of 2015, April 13 at Brilliant Sky Observatory, again with a telescope focal length setup of f/50. Five separate exposures of 1000 frames each were taken, along with a deconvolution star exposure and a drift angle exposure.

To obtain the best estimate for the camera angle for the Feb 18 observations, the drift exposure avi file was processed in REDUC to convert each frame to bmp files. These files were then examined using the REDUC Drift Analysis capability. While the Rigel exposures were a bit out of focus, a camera angle

was determined by selecting 43 separate beginning frames and ending frames used in the analysis to obtain a statistically sound camera angle.

Because the drift of Rigel across the field of view of the camera was nearly vertical, bottom to top, and because the exposure was a bit out of focus, the calculated camera angles from REDUC were either positive values (between 76.96° and 89.76°), or they were negative values (between -89.74° and -76.84°), depending on the pair of images selected for analysis, as shown in Figure 11 (REDUC Drift Analysis). Camera angles in REDUC are reported in values of 0° to 90° or 0° to -90° with respect to Celestial North. Therefore camera angles that would have a value $> 90^\circ$ are reported as negative values between 0° and -90° .

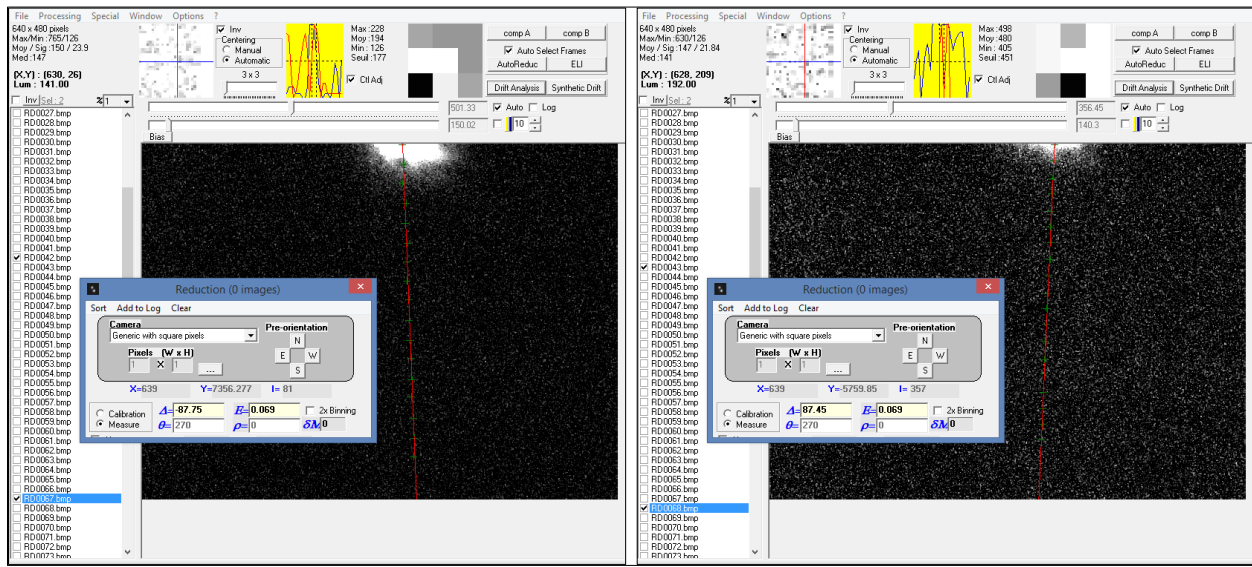


Figure 11: REDUC drift analysis screen shot examples. Rigel drift analysis for 2015 Feb 18 exposure.

The resulting distribution of all the camera angle estimates are shown in Figure 12 (Distribution of Raw REDUC Camera Angle Estimates), and show that any angle $> 90^\circ$ is reported in negative values.

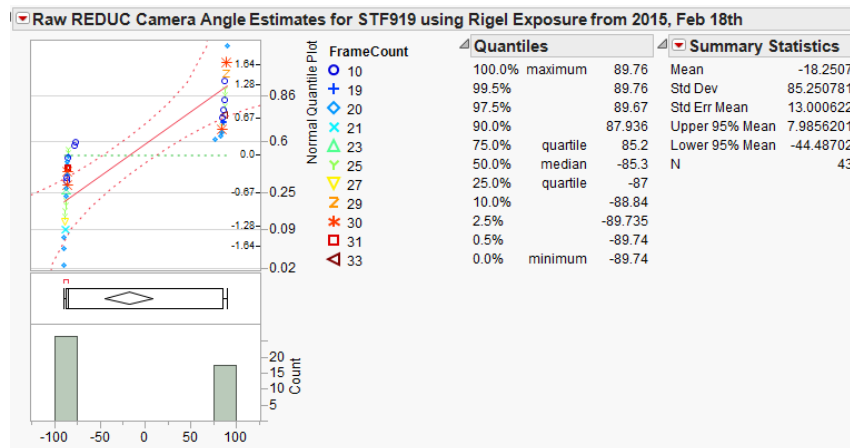


Figure 12: Distribution of raw REDUC camera angle estimates. Rigel drift analysis for 2015 Feb 18 exposure.

To normalize the distribution, and to obtain a statistically sound camera angle value, 180° was added to all camera angles with negative values. This normalized distribution is shown in Figure 13 (Normalized Distribution of REDUC Camera Angle Estimates).

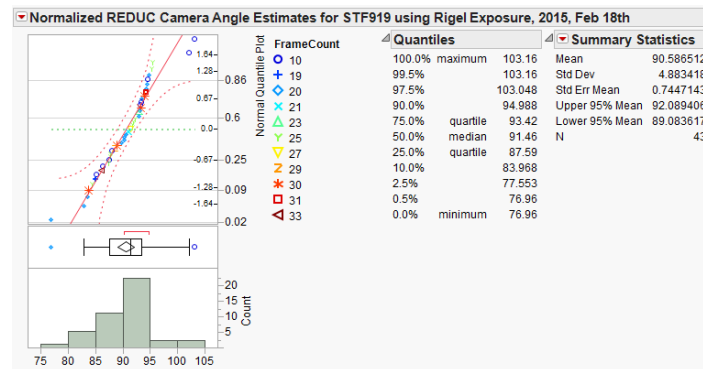


Figure 13: Normalized distribution of REDUC camera angle estimates. Rigel drift analysis for 2015 Feb 18th exposure.

Once the mean of the normalized distribution was found (90.587° , since it was $> 90^\circ$), the normalized value was then converted back to a standard value by subtracting 180° to obtain a final camera angle of -89.414° for the 2015 Feb 18 observations. STF919 was again observed on 2015 April 13 by Richard Harshaw, with a reported camera angle of -3.31° .

STF919 Plate Solve Analysis

The twelve observations and the deconvolution observation from Feb 18th were then converted from avi files to FITs files using REDUC, and then the FITs files were converted to PSD files in Plate Solve 3. The PSD files were then analyzed in Plate Solve using the Speckle Reduction function. The PSD files generated for the five April 13 observations were sent to author Ethan Wuthrich and were also analyzed in Plate Solve. For both the Feb 18 and the April 13 observations, the focal length used was f/50, so based on the calibration work that had been done, a pixel scale on $0.069''/\text{pixel}$ was used for all analysis.

Since all the observations contained the A, B, and C components of STF919, Plate Solve automatically picked light from the A component as the center point of each of the autocorrelograms generated for each observation. The software then allows for camera angle and pixel scale input. A target is then set over the B component, and then the rho and theta of B with respect to A is calculated by the software, and the data is recorded. The target is then removed and re-set over the C component, to get the theta and rho values of C with respect to A, and the data is recorded. Along with the theta and rho values, the center pixel location of the A, B, and C components were obtained and recorded. Values were saved to a residual table generated by Plate Solve.

Plate Solve does not contain a method to directly calculate the rho and theta between the B and C components, so these values were obtained by using a spreadsheet and basic trigonometry, based on the pixel locations recorded for each component, the camera angle, and the pixel scale. These results are shown in Table 5.

STF919 Observation Results Compared to WDS Historic Data

The residuals for rho and theta estimates done in Plate Solve 3 were then analyzed in JMPTM statistical software, and plotted with the historical WDS data. Not enough data was available to create an orbital plot, but current results can be compared to historic results.

When the observation data is compared to the historical data (see Figure 14), it is quickly apparent that the observational data values are not matched to the historical data values. A breakdown of the relations of the AB, AC, and BC components follows.

STF919 f/50; Camera Angle -89.41348; Pixel Scale = 0.069; Observation Date = 2015 Feb 18th (2015.13); Total Observations = 12						
	Values Calculated by PlateSolve 3				Manually Calculated Values	
	AB theta	AB rho	AC theta	AC rho	BC Theta	BC Rho
Average	136.166	7.164	129.873	9.885	113.966	2.875
STF919 f/50; Camera Angle -3.31; Pixel Scale = 0.069; Observation Date = 2015 April 13th (2015.28); Total Observations = 5						
	Values Calculated by PlateSolve 3				Manually Calculated Values	
	AB theta	AB rho	AC theta	AC rho	BC Theta	BC Rho
Average	136.618	7.154	129.820	9.910	113.036	2.931

Table 5: Summary of STF919 theta and rho calculations

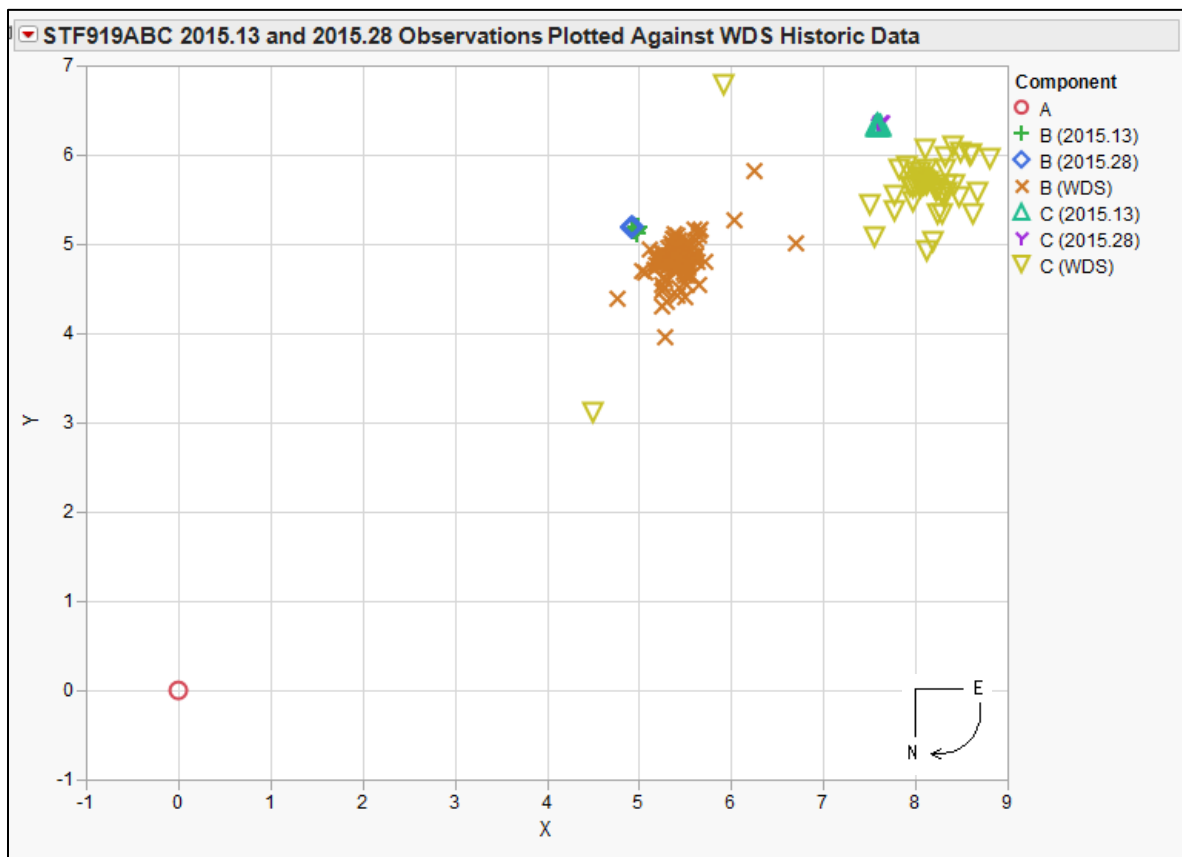


Figure 14: STF919ABC observations with historical WDS data

Figure 15 below shows a residual plot of the STF919AB latest observed data compared to historical WDS data.

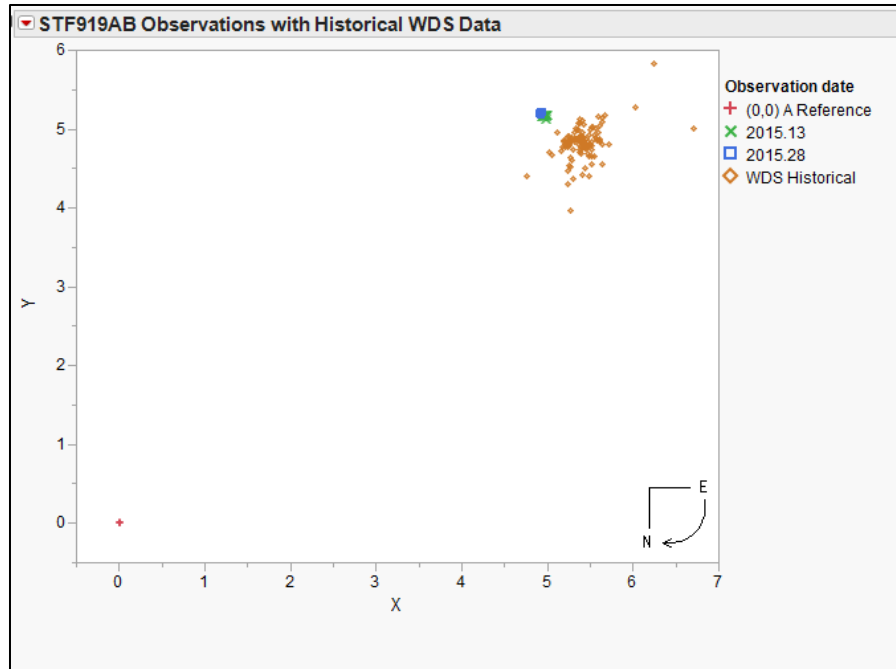


Figure 15: STF919AB observations with historical WDS data

The average theta values calculated for the STF919AB component are 136.166° for the 2015 February 18th (2015.13) observations and 136.618° for the 2015 April 13th (2015.28) observations compared to a historical value of approximately 132.7° . A plot of the theta values shows that the calculated angular separation is substantially different from the WDS historical data (see Figure 16). This data was collected over two observational sessions with a total of 17 different exposures. The camera angle calculation may play a part in the mismatch of the latest observational data compared to the historical data, but the method used to calculate the camera angle was the same method used on the STF1670 observations; those theta values were consistent with historical data values.

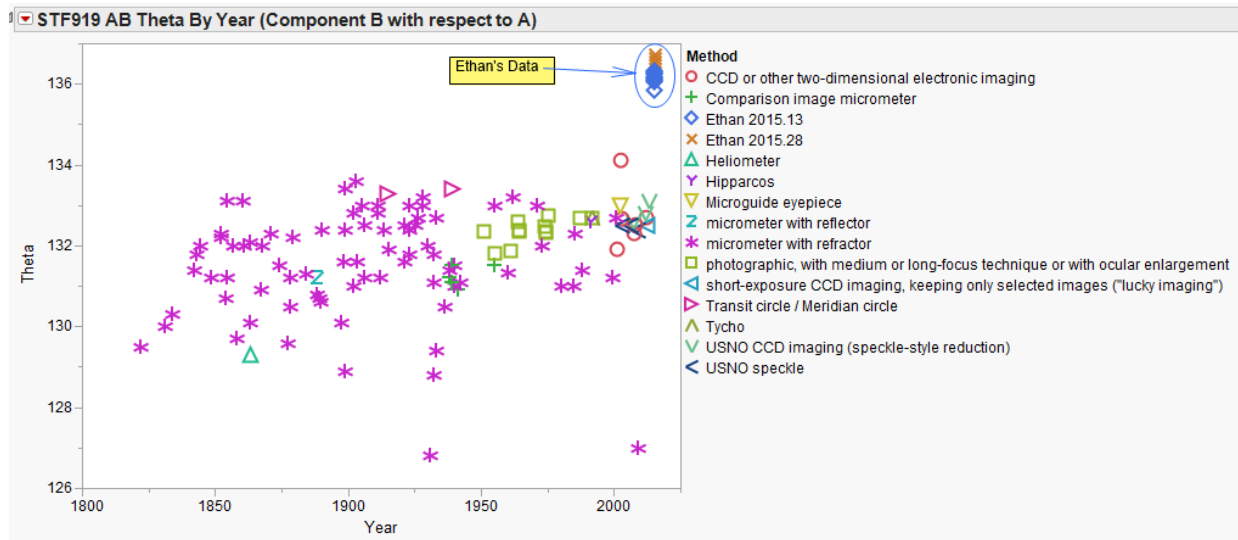


Figure 16: STF919AB theta values with historical WDS data by method of observation as a function of the years of observation.

The average rho values calculated for the AB component are 7.160" for the 2015.13 observations and 7.154" for the 2015.28 observations. These values agree with the historical WDS data. In particular, they are closely matched to previous CCD values and the USNO speckle values (see Figure 17). This indicates that the pixel scale values used were consistent with historical data.

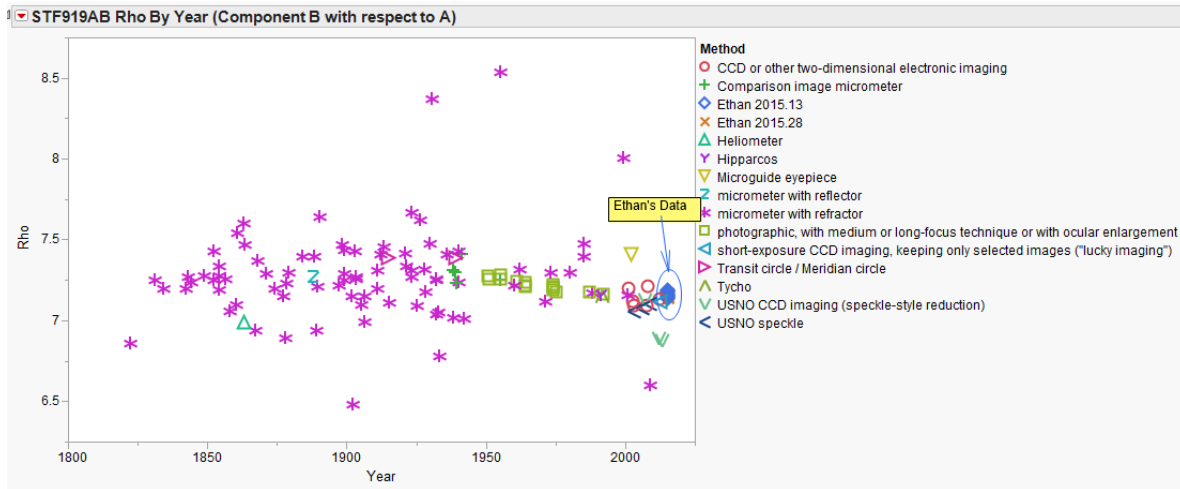


Figure 17: STF919AB rho values with historical WDS data by method of observation as a function of the years of observation

Similar to the STF919AB component, the STF919AC component shows a similar shift from the historical data as shown in the residual data plot in Figure 18.

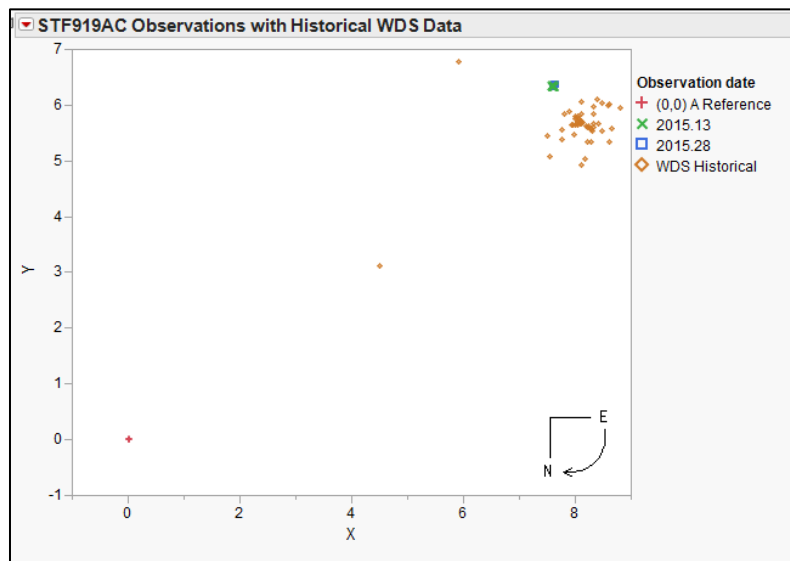


Figure 18: STF919AC observations with historical WDS data.

The average theta values calculated for the STF919AC component are 129.87° for the 2015.13 observations and 129.82° for the 2015.28 observations, compared to a historical value of approximately 125.6°. A plot of the theta values shows that the calculated angular separation is substantially different from the WDS historical data (see Figure 19). This data was collected over two observational sessions with a total

of 17 different exposures. The camera angle calculation may play a part in the mismatch of the latest observational data compared to the historical data, but the method used to calculate the camera angle was the same method used on the STF1670 observations; those theta values were consistent with historical data values.

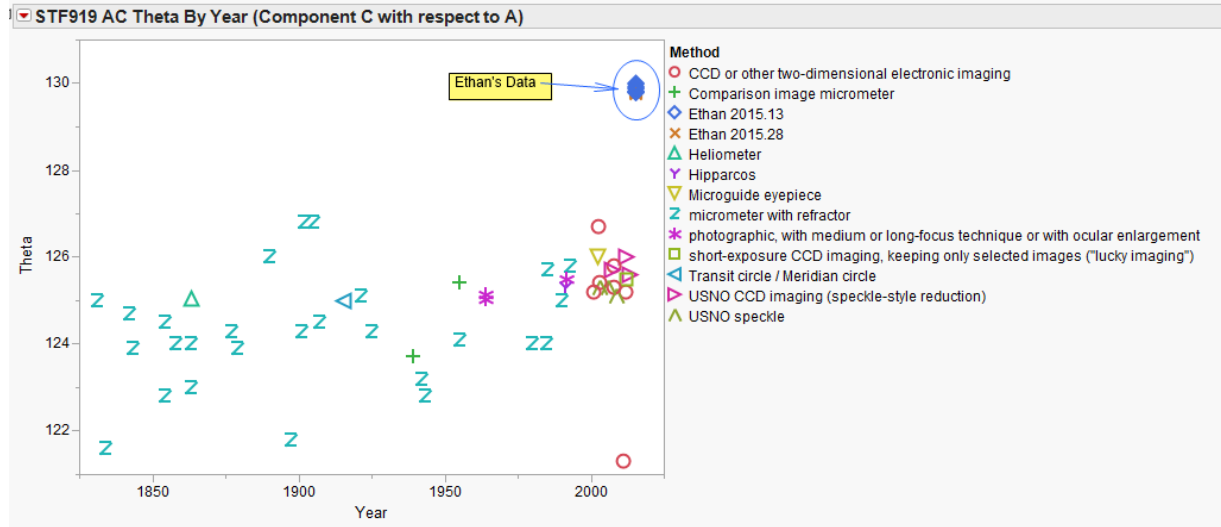


Figure 19: STF919AC theta values with historical WDS data by method of observation as a function of the years of observation.

The average rho values calculated for the AC component are 9.88" for the 2015.13 observations and 9.91" for the 2015.28 observations. These values agree with the historical WDS data. In particular, they are closely matched to previous CCD imaging values and the USNO speckle values (see Figure 20). This indicates that the pixel scale value

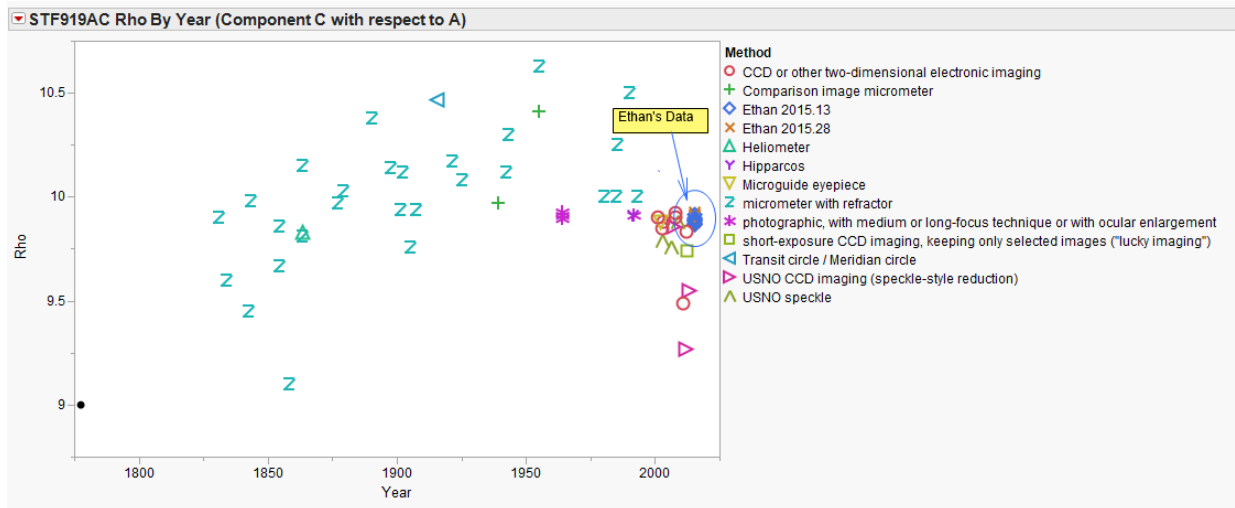


Figure 20: STF919AC rho values with historical WDS data by method of observation as a function of the years of observation.

Similar to the STF919AB and STF919AC components, STF919BC shows a similar shift from the historical data as shown in the residual data plot in Figure 21.

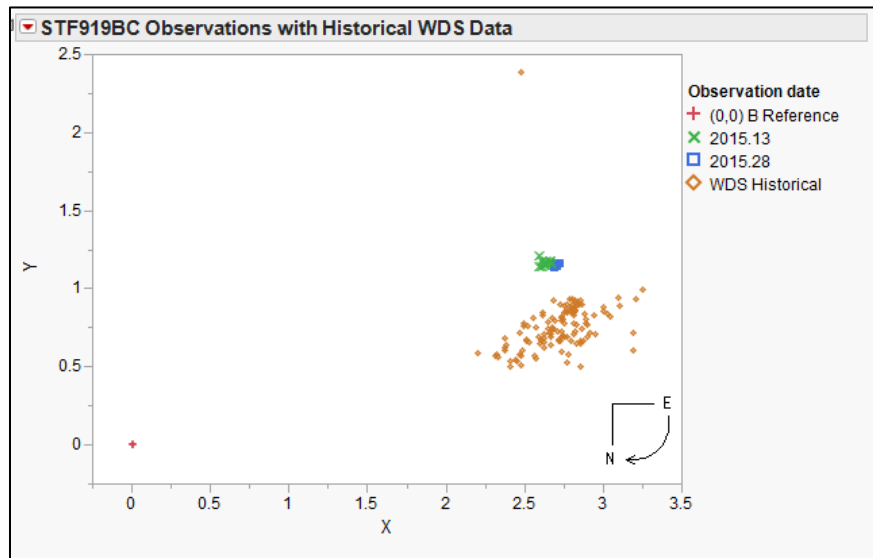


Figure 21: STF919BC observations with historical WDS data

The average theta values calculated for the STF919BC component are 113.966° for the 2015.13 observations and 113.036° for the 2015.28 observations, compared to a historical value of approximately 108° . A plot of the theta values shows that the calculated angular separation is substantially different from the WDS historical data (see Figure 22). This data was collected over two observational sessions with a total of 17 different exposures. The camera angle calculation may play a part in the mismatch of the latest observational data compared to the historical data, but the method used to calculate the camera angle was the same method used on the STF1670 observations; those theta values were consistent with historical data values.

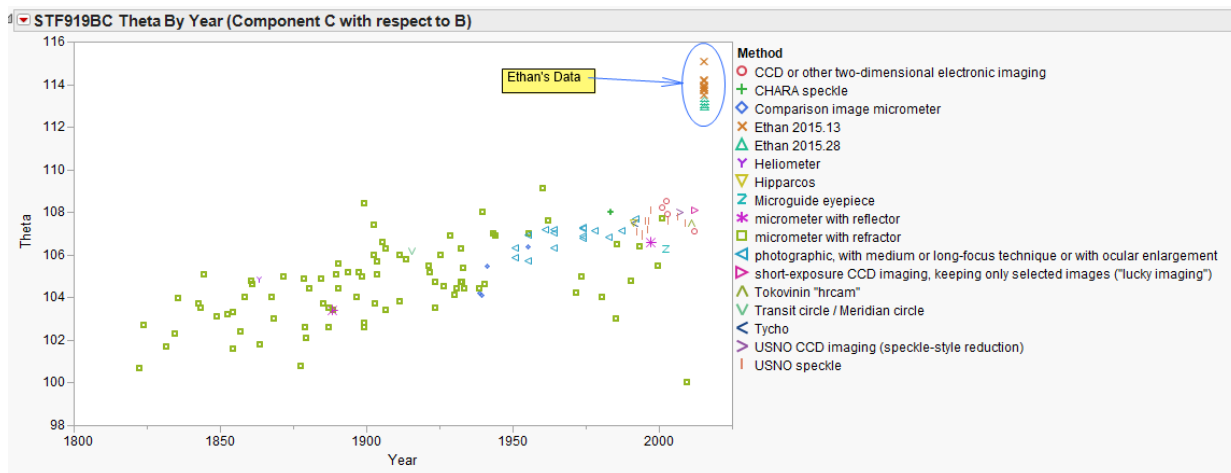


Figure 22: STF919BC theta values with historical WDS data by method of observation as a function of the years of observation.

The average rho values calculated for the BC component are $2.87''$ for the 2015.13 observations and $2.93''$ for the 2015.28 observations. These values agree with the historical WDS data. In particular, they are again closely matched to previous CCD imaging values and the USNO speckle values (see Figure 23). This indicates that the pixel scale values used were consistent with historical data.

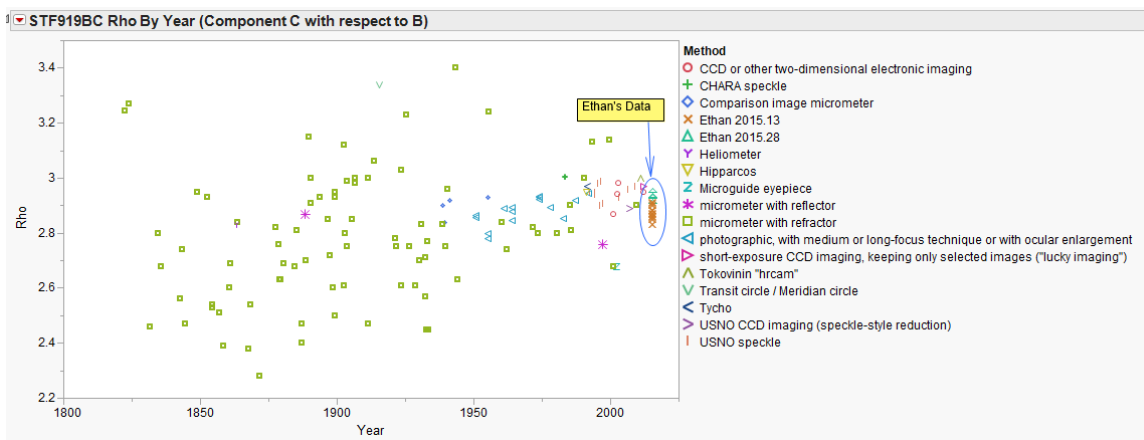


Figure 23: STF919BC rho values with historical WDS data by method of observation as a function of the years of observation.

Table 7 contains the average values for rho and theta for each of the observation nights:

STF919	Observations	AB theta	AB rho	AC theta	AC rho	BC Theta	BC Rho
2015.13	12	136.1661667	7.164425	129.8725833	9.884883333	113.9659255	2.874540073
2015.28	5	136.6182	7.154	129.8204	9.91022	113.0361502	2.931489715

Table 7: STF919 components observation dates and data summary.

Conclusion

The calculated theta and rho values for STF1670AB were consistent with historical data and trends.

The rho values for the STF919 components were consistent with historical trends, although the theta values did not appear to be. However, before the theta values are discounted, it should be pointed out that the data was collected over two observational sessions a month apart with multiple observations per session. The calculated theta values from these sessions did agree with each other.

WDS	System	focal length	Observation Date	Observations	AB theta	AB rho	AC theta	AC rho	BC Theta	BC Rho
06288-0702	STF919AB,AC,BC	f/50	2015.13	12	136.166	7.164	129.873	9.885	113.966	2.875
06288-0702	STF919AB,AC,BC	f/50	2015.28	5	136.618	7.154	129.820	9.910	113.036	2.931
12417-0127	STF1670AB	f/25	2015.276	5	4.961	2.1928				
12417-0127	STF1670AB	f/50	2015.276	3	5.503	2.0759				
12417-0127	STF1670AB	f/50	2015.28	5	6.9948	2.2941				

Table 8: STF919 and STF1670 Observation Summary.

The accuracy of the Celestron C-11 telescope and setup demonstrate that amateur use of speckle interferometry does hold promise.

Acknowledgements

Russell M. Genet (Cuesta College ASTR 299 Course Instructor), Jimmy Ray (Cuesta College ASTR 299 Course TA), Michael Mckelvy (Basha High Research Course Instructor), Randall Wuthrich (providing transportation, help and guidance, and acting as a consultant), Florent Losse (developed and provided latest beta version of REDUC software for use), Dave Rowe (developer of Plate Solve 3 software). This research has made use of the Washington Double Star Catalog maintained at the U.S. Naval Observatory.

References

- Argyle, R. W., ed. 2012. *Observing and Measuring Visual Double Stars*. 2nd ed. New York: Springer Science Business Media.
- Genet, R. 2015. *Introduction to Visual Double Star Research*. Webcast.
- Harshaw, R. 2015. Speckle Interferometry with Amateur Class Equipment. *The Society for Astronomical Sciences: Proceedings of the 34th Annual Symposium on Telescope Science*.
- Labeyrie, A. 1970. Attainment of diffraction limited resolution in large telescopes by Fourier analyzing speckle patterns in star images. *Astronomy and Astrophysics*. 6(1): 85-87.
- Pickering, W. H. 1923. The Real Uses of Astronomy, Sidereal and Planetary. *Popular Astronomy*. 32: 134-36.